Characterization of micro- to macroscopic response of polymers containing voids under macroscopically uniform deformation

Tomita, Yoshihiro

Wei, Lu

(Citation)
International Journal of Solids and Structures,39(13/14):3409-3428

(Issue Date)
2002-07

(Resource Type)
journal article

(Version)
Accepted Manuscript

(URL)
https://hdl.handle.net/20.500.14094/90000020

Characterization of Micro- to Macroscopic Response of Polymers Containing Voids Under Macroscopically Uniform Deformation

Yoshihiro Tomita and Wei Lu
Graduate School of Science and Technology,
Kobe University, Nada, Kobe, Japan 657-8501
Fax: +81-78-803-6125 E-mail address: tomita@mech.kobe-u.ac.jp

Abstract

For the characterization of mechanical characteristics of polymers containing voids (cavitated rubbery particles), a homogenization method has been developed, which can handle large deformation problems including the onset and propagation of instability and can reproduce the micro- to macroscopic deformation behavior of polymers with periodically distributed voids under macroscopically inhomogeneous loading conditions. A parametric study has clarified the characteristic features of polymers containing periodically distributed heterogeneous cylindrical voids of different volume fractions subjected to macroscopically homogeneous stress in different directions. Different types of shear bands are observed, depending on the tensile direction with respect to the unit cell. The shear band connecting the voids that appear in the early stages of deformation is responsible for the macroscopic yielding. Increasing the volume fraction of the voids results in a decrease in the macroscopic yield stress and in the directional dependence of the macroscopic stress-strain relationship. The moderate heterogeneity of voids causes complicated and different types of shear bands; however, due to the high stress concentration caused by the presence of small voids, the onset and propagation of the shear bands are promoted, and the macroscopic stress-strain relationships become essentially isotropic. Nevertheless, the volumetric strain of unit cell changes with volume fraction and heterogeneity of the voids and tension directions.

1. Introduction

Blending with 10 to 40% volume fraction of second-phase particles, conventional rubber particles, ranging in size from 0.1 to 10 μm, is commonly adopted in order to control the mechanical properties of a polymer. It has been clarified that the cavitation of second-phase particles leads to a porous matrix in which triaxiality next to the void is substantially decreased, which suppresses the onset of crazing and promotes plastic shear deformation in the materials (Yee, 1977, Fukui, et al., 1991, Society of Polymer Science, Japan 1991, Steenbrink and van der Giessen, 1997). Due to the increase in energy dissipation inside the plastic deformation region, the toughness of the glassy polymer is considerably enhanced.

In order to clarify the deformation behavior of blended polymers, computational studies have been performed. Among them, computational simulations employing realistic constitutive equations of polymers (Boyce et al., 1988, Arruda and Boyce, 1993, Wu and van der Giessen, 1993, Tomita et al., 1997, Tomita and Adachi, 1998, Tomita et al., 1999) have been carried out (Steenbrink and van der Giessen, 1997, 1998, 1999, Smit et al., 1999, Tanaka et al., 2000, Socrate and Boyce, 2000, Pijnenburg and van der Giessen, 2001, Tomita and Lu, 2001) and the mechanisms for improving the mechanical characteristics of polymers upon blending of second-phase particles, i.e., rubber particles, have been investigated. However, often the computational study of the blended materials is restricted to unit cells that deform under simple loading processes (Steenbrink and van der Giessen, 1997, 1998, 1999, Tanaka et al., 2000, Socrate and Boyce, 2000). The representative volume element method was employed for a large number of voids with random distribution and the effects of the volume fraction and distribution of the voids on the macroscopic response were discussed (Smit et al., 1999). Very recently, discussions associated with nonsymmetrical deformation behavior of unit cells containing voids of identical size (Pijnenburg and van der Giessen, 2001) and compressible particles of different sizes (Tomita and Lu, 2001) were presented.

To clarify the mechanical aspect and provide a quantitative picture with respect to the mechanisms for improving the mechanical characteristics of blended materials, the homogenization method used for the linear elastic problem (Guedes and Kikuchi, 1990) is extended to large deformation problems including the onset and propagation of instabilities. This method can reproduce the micro- to macroscopic deformation behavior of blended polymers with periodically distributed second-phase rubber particles under macroscopically inhomogeneous loading conditions. A parametric study has been performed by means of a series of simulations for a plane strain glassy polymer containing periodically distributed heterogeneous cylindrical voids which represented the cavitated rubber particles of different volume fractions under macroscopically homogeneous stress. In particular, we address the effect of heterogeneity of the voids and the tension directions with respect to the periodically distributed voids on the micro- to macroscopic response.

2. Constitutive Equations

In order to describe the experimentally observed characteristic hardening feature of the glassy polymers, the molecular chain network model has been developed by Boyce et al. (1988) and subsequently, further modifications have been carried out (Arruda and Boyce, 1993, Wu and van der Giessen, 1993, Tomita et al., 1997, Tomita and Adachi, 1998, Tomita et al., 1999). The corresponding three-dimensional constitutive equation in the updated Lagrangian expression can be derived along the same lines as discussed by Boyce et al. (1988), in which the plastic strain rate $\dot{\varepsilon}_{ij}^{p}$ is expressed as

$$\dot{\varepsilon}_{ij}^{p} = \frac{\dot{\gamma}^{p}}{\sqrt{2}\tau}\hat{\sigma}'_{ij}\ ,\quad \tau = \left(\hat{\sigma}'_{ij}\hat{\sigma}'_{ij}/2\right)^{1/2},\quad \hat{\sigma}_{ij} = \sigma_{ij} - B_{ij} \tag{1}$$

where σ_{ij} is the Cauchy stress and B_{ij} is the back-stress tensor which will be further specified later.

The shear strain rate $\dot{\gamma}^{p}$ in Eq. (1) is given by Argon (1973) as:

$$\dot{\gamma}^{p} = \dot{\gamma}_0 \exp\left[\left(-\frac{As_0}{T}\right)\left\{1-\left(\frac{\tau}{s_0}\right)^{5/6}\right\}\right], \tag{2}$$

where $\dot{\gamma}_0$ and A are constants, T is the absolute temperature, $s_0 = 0.077G/(1-\nu)$ is the athermal shear strength, G is the elastic shear modulus, ν is Poisson's ratio and τ is the applied shear stress. Boyce et al. (1988) extended this expression to include the effect of pressure p. They used $s + ap$ instead of s_0, where s is the shear strength which changes with plastic strain from s_0 to a stable value s_{ss}, p is the pressure and a is a pressure-dependent coefficient. Since s depends on the temperature and strain rate, the evolution equation of s can be expressed as $\dot{s} = h\left\{1-\left(s/s_{ss}\right)\right\}\dot{\gamma}^{p}$ where h is the rate of

resistance with respect to plastic strain. See Arruda et al. (1995) for the case of temperature dependence of the strain hardening of polymer.

The principal components of the back-stress tensor B_i for the eight-chain model (Arruda and Boyce, 1993), which is widely used in computational simulations, are

$$B_i = \frac{1}{3} C^R \sqrt{N} \frac{V_i^2 - \lambda^2}{\lambda} L^{-1}\left(\frac{\lambda}{\sqrt{N}}\right),$$

$$L(x) = \coth x - \frac{1}{x}, \quad \lambda^2 = \frac{1}{3}(V_1^2 + V_2^2 + V_3^2), \tag{3}$$

where V_i is the principal plastic stretch, $\lambda_L = \sqrt{N}$ is the locking stretch, i.e., limiting stretch in tension, N is the average number of segments in a single chain, $C^R = nkT$ is a constant, n is the number of chains per unit volume, k is Boltzmann's constant, and L is the Langevin function. In the eight-chain model (Arruda and Boyce, 1993) and other models (Boyce et al., 1988, Arruda and Boyce, 1993, Wu and van der Giessen, 1993), the number of entangled points of molecular chains is assumed to be fixed during the deformation, and the average number of segments, N, is constant. Therefore, these models are referred to as affine models. To accommodate the change in the entanglement situation due to deformation and temperature change, a nonaffine model has been proposed (Tomita and Tanaka 1995, Tomita et al., 1997, Tomita and Adachi, 1998) in which the change in the number of entangled points is taken into account. The simplest expression of the number of entangled points m in the temperature- independent case becomes

$$m(\xi) = m_0\{-c(1-\xi)\}. \tag{4}$$

The variable ξ represents the local deformation of polymeric material (Tomita et al., 1997). m_0 is the number of entangled points at the reference temperature $T = T_0$ and the initial state of deformation $\xi = 1$; c is a material constant. The decrease in ξ causes a reduction in the number of entangled points m. Correspondingly, the average number of segments in a single chain increases, which results in enhanced extensibility of the material.

The complete elastoplastic constitutive equation can be established by introducing the constitutive equation for the elastic part of the strain rate. The final constitutive equation that relates the rate of Kirchhoff stress $\dot{S}_{ij}$ and strain rate $\dot{\varepsilon}_{kl}$ becomes

$$\dot{S}_{ij} = L_{ijkl}\dot{\varepsilon}_{kl} - P'_{ij}, \quad L_{ijkl} = D^e_{ijkl} - F_{ijkl}$$

$$F_{ijkl} = \frac{1}{2}\left(\sigma_{ik}\delta_{jl} + \sigma_{il}\delta_{jk} + \sigma_{jl}\delta_{ik} + \sigma_{jk}\delta_{il}\right), \quad P'_{ij} = D^e_{ijkl}\frac{\dot{\gamma}^p}{\sqrt{2}\tau}\hat{\sigma}'_{kl}, \tag{5}$$

where D^e_{ijkl} is the elastic stiffness tensor.

3. Computational Strategies

In order to estimate the micro- to macroscopic deformation behavior of a blended polymer containing the second phase, rubber particles that are assumed to be distributed periodically, the homogenization method (Guedes and Kikuchi, 1990) is extended, along the same lines as indicated for the viscoplastic case (Wu and Ohno, 1999), to the present problem formulated using an updated Lagrangian expression (Hill, 1958, Kitagawa et al. 1972).

Consider the two-dimensional (2D) problem shown in Fig.1, with domain Ω and boundary S subjected to surface force P_i on S_t and prescribed velocity on S_u. The body is formed by the spatial repetition of a base cell Y made of different materials. Assuming that the base cell is very small, of order η compared with the dimensions of the entire body, the global coordinate is x_i for the entire body and the local coordinate is y_i related to the single base cell, then $y_i = x_i / \eta$. Similar to the assumption used in the case of linear elastic materials (Guedes and Kikuchi, 1990), the velocity v_i is presumed to be expressed as an asymptotic expansion with respect to parameter η.

$$v_i(x,y) = v_i^0(x) + \eta v_i^1(x,y) + \eta^2 v_i^2(x,y) + ... \tag{6}$$

where $v_i^0(x)$ is the microscopically uniform part of velocity, whereas $v_i^1(x,y), v_i^2(x,y), ...$ are Y-periodic and local perturbations due to the presence of heterogeneities in the unit cell. The velocity gradient $v_{i,j}$ and strain rate $\dot{\varepsilon}_{ij}$ are expressed as

$$v_{i,j} = \frac{\partial v_i}{\partial x_j} + \frac{1}{\eta}\frac{\partial v_i}{\partial y_j}, \quad \dot{\varepsilon}_{ij} = \frac{1}{2}\left(v_{i,j} + v_{j,i}\right) \ . \tag{7}$$

Substituting the velocity v_i into Eq.(7), we have the expression of strain rate

$$\dot{\varepsilon}_{ij}(x,y) = \eta^{-1}\dot{\varepsilon}_{ij}^0 + \eta^0\left\{\dot{E}_{ij}^0 + \dot{\varepsilon}_{ij}^1\right\} + \eta^1\left\{\dot{E}_{ij}^1 + \dot{\varepsilon}_{ij}^2\right\} + ... \tag{8}$$

$$\dot{E}_{ij}^k = \frac{1}{2}\left(\frac{\partial v_i^k}{\partial x_j} + \frac{\partial v_j^k}{\partial x_i}\right), \dot{\varepsilon}_{ij}^k = \frac{1}{2}\left(\frac{\partial v_i^k}{\partial y_j} + \frac{\partial v_j^k}{\partial y_i}\right)$$

Introducing thus obtained velocity, velocity gradient and strain rate into the virtual work principle (Hill, 1958, Kitagawa et al., 1972) with the constitutive equation (Eq.(5)) and rearranging at the same order η, we arrive at the virtual work principle for a macroscopic body:

$$\int_\Omega \left[L_{ijkl}^H \dot{E}_{kl}^0 - P_{ij}^H + \sigma_{ij}^H + \tau_{ijkl}^H \frac{\partial v_k^0}{\partial x_l} \right] \frac{\partial \delta v_i}{\partial x_j} d\Omega = \int_{S_t} \dot{P}_i \delta v_i dS \tag{9}$$

$$
\left.
\begin{aligned}
L^H_{ijkl} &= \frac{1}{|Y|}\int_Y \left[L_{ijkl} - L_{ijpq}\frac{1}{2}\left(\frac{\partial \chi^{kl}_p}{\partial y_q} + \frac{\partial \chi^{kl}_q}{\partial y_p} \right) \right] dY \\
P^H_{ij} &= \frac{1}{|Y|}\int_Y \left[P'_{ij} - L_{ijkl}\frac{1}{2}\left(\frac{\partial \phi_k}{\partial y_l} + \frac{\partial \phi_l}{\partial y_k} \right) \right] dY, \\
\sigma^H_{ij} &= \frac{1}{|Y|}\int_Y \sigma_{mj}\frac{\partial \phi_i}{\partial y_m} dY, \\
\tau^H_{ijkl} &= \frac{1}{|Y|}\int_Y \left[\sigma_{lj}\delta_{ki} - \sigma_{mj}\frac{\partial \chi^{kl}_i}{\partial y_m} \right] dY
\end{aligned}
\right\} \tag{10}
$$

$$
\dot{\varepsilon}^0_{ij} = \dot{E}^0_{ij} - \frac{1}{2}\left(\frac{\partial \chi^{kl}_i}{\partial y_j} + \frac{\partial \chi^{kl}_j}{\partial y_i} \right)\dot{E}^0_{kl} + \frac{1}{2}\left(\frac{\partial \phi_i}{\partial y_j} + \frac{\partial \phi_j}{\partial y_i} \right) \tag{11}
$$

$$
\dot{S}^0_{ij} = L_{ijkl}\dot{\varepsilon}^0_{kl} - P'_{ij} \tag{12}
$$

In Eq.(10) $|Y|$ indicates the area of the unit cell shown in Fig.1.

Equations (9), (10) and (11), (12) are the governing equations for the macroscopic and microscopic scales, respectively. The notations χ^{kl}_p and ϕ_k are characteristic functions defined in the unit cell, which satisfy the Y periodicity and are determined by the following equations.

$$
\int_Y \left[L_{ijpq}\frac{1}{2}\left(\frac{\partial \chi^{kl}_p}{\partial y_q} + \frac{\partial \chi^{kl}_q}{\partial y_p} \right) + \sigma_{qj}\delta_{pi}\frac{\partial \chi^{kl}_p}{\partial y_q} \right] \frac{\partial \delta v_i}{\partial y_j} dY = \int_Y \left(L_{ijkl} + \sigma_{lj}\delta_{ki} \right) \frac{\partial \delta v_i}{\partial y_j} dY \tag{13}
$$

$$
\int_Y \left[L_{ijkl}\frac{1}{2}\left(\frac{\partial \phi_k}{\partial y_l} + \frac{\partial \phi_l}{\partial y_k} \right) + \sigma_{mj}\frac{\partial \phi_i}{\partial y_m} \right] \frac{\partial \delta v_i}{\partial y_j} dY = \int_Y P'_{ij}\frac{\partial \delta v_i}{\partial y_j} dY \tag{14}
$$

Thus, characteristic functions χ^{kl}_p and ϕ_k for the unit cell depend solely on the material characteristics and configuration of the microstructure of the unit cell, which are, in turn, obtained without interacting stress and strain of the macroscale. On the other hand, the macroscopic equilibrium given by Eq. (9) can be solved independently because the macroscopic characteristic functions indicated in Eq. (10) are identified through Eqs. (13) and (14). The homogenized material characteristics indicated by Eq. (10) reflect the volume fraction, size and distribution of second-phase-particle-dependent onset and propagation of the shear band in the unit cell. Once the average stress rate is estimated, different types of stress rates can be obtained using the same transformation rule on the microscale (Ohno and Okumura, 1999). Equation (9) can be applied to solve the general boundary value problems

for the materials with periodic microstructures under macroscopically nonuniform deformation. In the present investigation, we use Eq.(9) for clarification of the deformation behavior of a unit cell under macroscopically uniform deformation.

4. Computational Model

A typical rubber-blended PC contains rubber particles which are spherical with μm length scale and are dispersed throughout the matrix. The mechanical characteristics of the blended material are strongly dependent on the initiation and propagation of the shear band in the matrix polymer and the cavitations of rubber particles, which are strongly affected by the volume fraction and size of rubber particles. Although the distribution of the rubber particles is somewhat random, here, we assume that it is periodic and evaluate the detailed characteristics of microscopic deformation and clarify their effect on the macroscopic mechanical characteristics of the blended polymer. The discussions are focused on the essential feature of the voids, namely cavitated rubbery particles, containing polymer.

Figure 2 illustrates the computational model in which heterogeneous voids are assumed to be distributed periodically. Here, the matrix satisfies the constitutive equation (Eq.(5)). Each quadrilateral corresponds to a cross-triangular element. As indicated in Fig. 2, in the present investigation, the heterogeneous voids are assumed to be circular cylinders of radii of curvature r_1 and r_2 contained in the unit cell with side lengths w_0 and l_0, which characterizes the cases that will be investigated. The boundary conditions on the macroscopic scale are that the upper and bottom surfaces are shear-free with a constant displacement constraint, whereas the right and left surfaces are assumed to be stress-free. In the present analysis thus developed homogenization method is employed, and the boundary condition for macroscopic scale is easily introduced as in the conventional problems without the additional boundary condition for the unit cell. Therefore, the plane strain analyses with off principal directional tension with respect to unit cell are straightforward as compared with other unit cell methods (Pijnenburg and van der Giessen 2001). It should be noted that this cannot be carried out in the axisymmetric approximation that is used for 3D cells (Steenbrink and van der Giessen, 1999, Socrate and Boyce, 2000) or for more elaborated stacked hexagonal 3D cells (Socrate and Boyce, 2000). Extensions of these models to account for the case with the heterogeneous voids would be very difficult. The discussion on comparisons between these models is given by Socrate and Boyce (2000). On the other hand, the localized patterns in a randomly voided polymer are very complex as approximated by 2D simulation (Smit et al., 1999), which is available by sacrificing the resolution of deformation behavior in microscopic scale.

In order to investigate the effect of the loading direction on the principal direction of the unit cell, namely, the y_2 coordinate, the angle θ, which is the angle of the tension direction with respect to the principal direction of the unit cell, is introduced and is

parametrically varied from 0 to 45 degrees. It is important to note that the constitutive models used do not have a material length scale. Thus, the only length scales in the problem are the cell dimensions which govern the solution through the dimensionless variables r_1 / r_2, l_0 / w_0 and volume fraction f_0.

Here we will discuss the effects of volume fraction f_0, the size of voids r_1 / r_2 with $l_0 / w_0 = 1$ and the direction θ on such macroscopic deformation behavior as the average stress-strain relationship and microscopic deformation behavior such as onset and propagation of the shear band and mean stress distribution.

For a typical unit cell, which is the microscopic element of the blended material, a macroscopically homogeneous strain rate $\dot{\varepsilon}_0 = 10^{-5} / s$ is applied. The material parameters for the polymer employed are $E / s_0 = 23.7$, $s_{ss} / s_0 = 0.79$, $h / s_0 = 5.15$, $As_0 / T_0 = 78.6$, $\alpha = 0.08$, $\dot{\gamma}_0 = 2.0 \times 10^{15} / s$, $s_0 = 97 MPa$, $T_0 = 296 K$, $m_0 = 7.83 \times 10^{26}$ and $c = 0.33$ (Tomita et al. 1997, Tomita and Adachi, 1998) which were the modified versions of those for the affine-type 8-chain model (Arruda and Boyce, 1993, Wu and van der Giessen, 1993).

5. Computational Results and Discussion

Here, the problems associated with the heterogeneity and volume fraction of the voids-dependent microscopic to macroscopic deformation behavior of a polymer with voids are investigated by employing the computational model presented in section 4.

5.1 Average stress-strain relationship for a unit cell

Figure 3 shows the typical nominal stress and volumetric strain for unit cell versus nominal strain relationships for polymers containing voids of sizes $r_1 / r_2 = 1, 2, 5$ and volume fractions $f_0 = 0.2$ under uniaxial tension with different directions $\theta = 0^\circ, 15^\circ, 30^\circ, 45^\circ$. The response in the case of identical void size exhibits considerable anisotropy, particularly in yield stress and around yield points, depending on the direction. Macroscopic yield stress and stress corresponding to the strain over yielding point for $\theta = 30^\circ, 45^\circ$ are higher than those for $\theta = 0^\circ, 15^\circ$. In contrast, macroscopic yield stress decreases for the case of different void sizes, $r_1 / r_2 = 2$ and the macroscopic responses are nearly isotropic for all deformation processes investigated here. It is noted that the macroscopic yield stress is essentially identical to this case. These typical characteristics are seen in the case with $r_1 / r_2 = 5$ in which, as opposed to the cases with $r_1 / r_2 = 1, 2$, yield stress for $\theta = 0^\circ, 15^\circ$ is higher than that for $\theta = 30^\circ, 45^\circ$. The discussion concerning the stress-strain relationship and the deformation characteristics in the unit cell is given in section 5.2. These results suggest that the inclusion of voids of moderately different sizes has a tendency to result in materials exhibiting macroscopically isotropic responses. Due to the existence of the voids, the resistance to deformation of the material does not exhibit the remarkable drop that can be seen in polymer without voids, which is attributable to the contribution of the voids to the promotion of orientation hardening successively in the ligament area of the matrix polymer.

5.2 Onset and propagation of shear band in unit cell

The equivalent strain rate distributions are shown in Fig. 4 with four different deformation levels of $u/L = 0.025,\ 0.050,\ 0.100$ and 0.150. Figure 4 (a) $\theta = 0$ with $r_1/r_2 = 1$, shows the typical onset and propagation behaviors of the shear band. The high- strain-rate region emanates from the equator of the particle and then localizes into a "wing-type" shear band, as termed by Steenbrink and van der Giessen (1997), which develops into multiple bands. The corresponding stress-strain relationship in Fig. 3 (a) exhibits an inflection at the point where the wing-type shear band developed. Subsequently, the orientation hardening in the core of the shear band starts so that the rate of deformation at the center of the band decreases. The front of the sheared region advances as multibands of high strain rate, and propagates towards the top and bottom parts of the unit cell. For the case with $\theta = 15^\circ$, a very strong shear band that connects the voids appears with relatively small deformation, which is associated with the decrease of the yield points, as indicated in Fig. 3 (a). Then the front of the sheared region advances as two bands to undeformed regions while preserving the same pattern. Increasing the angle to $\theta = 30^\circ$, high-strain-rate regions appear near the surface of the voids and they connect with the nearest particles at 45 degrees with respect to the tension direction, and subsequently, a new weak shear band at 45 degrees with respect to the tension direction develops and connects particles. Then shear bands move along the particle surface and align. With further deformation, shear bands again start to misalign, which causes additional distortion of the voids. In the case of $\theta = 45^\circ$, the high-strain-rate regions that appear near the surface of the voids and the midpoint between two voids connect, forming wing-type shear bands. In the later stage of deformation, cross-type shear bands appear on the ligament and develop. For $\theta = 15^\circ, 30^\circ$, the characteristic features of shear band patterns partially share those in the cases of $\theta = 0^\circ, 45^\circ$.

The strain rate distribution in the case of voids of different sizes is shown in Fig. 4 (b). For $\theta = 0^\circ, 15^\circ$, as indicated, wing-type shear bands emanate from the surface of the small voids; whereas they start from the surface of large voids in the cases of $\theta = 30^\circ, 45^\circ$. Subsequently, the shear band connects large voids via small voids. Most of the typical characteristic features of the onset and propagation of the shear band in the case of uniformed void size are preserved, except in the case of $\theta = 45^\circ$. Within the calculated deformation range, no shear bands connecting the small voids were observed.

As we increase the size difference between particles to $r_1/r_2 = 5$, the typical characteristic features for $r_1/r_2 = 2$ are preserved. The shear bands connecting the large voids via small voids developed in the cases of $\theta = 0^\circ, 15^\circ$, while the shear bands directly connecting the large particles developed in the cases of $\theta = 30^\circ, 45^\circ$. In the former cases, propagation of shear bands along the small voids causes significant distortion of the voids. The onset and development of the wing-type shear band on the ligament causes the decrease in the stress in the later stages of deformation as seen in the case of $\theta = 0^\circ$. Within the range

of deformation simulated in the present investigation, no strong shear bands connecting small particles were observed in the cases of $\theta = 30^\circ, 45^\circ$. These different characteristic features cause the differences in the macroscopic yield stress values, as mentioned previously, and in the macroscopic deformation behaviors. That is, the average stress-strain relationships for $\theta = 0^\circ, 15^\circ$ and $r_1 / r_2 = 1$ approximately correspond to those for $\theta = 45^\circ, 30^\circ$ and $r_1 / r_2 = 5$. In these cases, the deformation behaviors are essentially the same.

5.3 Deformation of voids

The distortion and rotation of the voids shown in Figs. 5 and 6 are governed by the onset and propagation of the shear band connecting the voids. The strong distortions of the void shape are seen in Fig. 5 and correlate with the shear bands shown in Fig. 4. Figure 6 shows that the rotation of large voids is different from those of identical sized voids and small voids which largely rotate as compared with the large voids. In addition, the rotation of the voids is strongly affected by the connection of the shear band, which is typically seen in the rotation of the small voids as shown in Fig. 6 for the case of $\theta = 15^\circ$ and $r_1 / r_2 = 5$. The rate of rotation of the small voids remarkably increases as the shear band connecting large voids via small voids develops and propagates along the small void over $u / L = 0.02 - 0.08$ and it decreases as the shear band propagates away from the small voids. Similar behavior can be seen in the case of $r_1 / r_2 = 2$. Interestingly, the rotation rate of the large void for $r_1 / r_2 = 5$ is high before the shear band connecting large voids via small voids develops and after which, it decreases.

5.4 Volumetric Strain

To characterize the dilatancy of the blended polymer, the volumetric strain for a unit cell is shown. Figure 3 indicates the plot of volumetric strain for a unit cell versus nominal strain for the cases of $f_0 = 0.2$, $r_1 / r_2 = 1, 2, 5$ and $\theta = 0^\circ, 15^\circ, 30^\circ, 45^\circ$. Depending on the heterogeneity of the voids and tension directions, quite different responses are seen. The rate of the evolution of volumetric strain for the case with $\theta = 15^\circ, 30^\circ$ is higher than those for $\theta = 0^\circ, 45^\circ$ except $r_1 / r_2 = 1$, in which the rate for $\theta = 45^\circ$ maintains the same level as those for $\theta = 15^\circ, 30^\circ$. Furthermore, the rapid increase of volumetric strain for $\theta = 0^\circ$ and $r_1 / r_2 = 5$ is noted in the later stage of deformation. The prediction of average volumetric strain due to V-BCC Model and SHA Model (Socrate and Boyce, 2000) for $f_0 = 0.2$ exhibits similar tendencies which are seen in the cases of $\theta = 0^\circ, 45^\circ$, respectively. The heterogeneity of the void size causes the decrease in the dilatancy and anisotropic response. Therefore, the results suggest the difficulty of establishing the isotropic constitutive equation for the blended polymer.

The volumetric strain of voids due to the deformation is seen in Fig. 7. For $r_1 / r_2 = 1$, $\theta = 15^\circ, 30^\circ, 45^\circ$, the continuous increase of void volume change is seen, whereas, it exhibits saturation in the case of $\theta = 0^\circ$, which results in the characteristic feature of volumetric strain of the unit cell as shown in Fig. 3. For the heterogeneous voids case, despite

the complicated behavior of small voids due to the onset and propagation of shear bands as indicated in Fig.4, the volumetric change of large voids essentially governs the dilatation of the voided polymer.

5.5 Mean stress

The mean stress, particularly positive mean stress, is the essential parameter for predicting the onset of crazing. Therefore, here we will discuss the local distribution of mean stress in unit cell. Figure 8 shows the typical distribution of the mean stress for the cases of $f_0 = 0.2$, $r_1 / r_2 = 2$ and $\theta = 0^\circ, 30^\circ$. For comparison purposes, the strain rate distributions are also shown. Table 1 shows the maximum values of the mean stress normalized by shear strength s_0 for the different deformation stages for $r_1 / r_2 = 1, 2, 5$ and $f_0 = 0.2$. The maximum value of the mean stress attains a very high value at macroscopic yield point, then decreases due to softening and again increases due to orientation hardening. In the early stages of deformation, high positive mean stress appears near the boundary surface of the voids at the equator with respect to the tension direction. As the deformation increases, the location of the high mean stress point moves into the interior part and then its value decreases due to the onset and propagation of shear band at a different position. The increase of the heterogeneity of the voids causes the decrease of the maximum mean stress over relatively small strain range. The local maximum mean stress at macroscopic yielding under uniaxial plane strain tension (result reported by Socrate and Boyce (2000) by using the V-BCC Model with $f_0 = 0.25$ and triaxiality $1/\sqrt{3}$) is approximately $0.54 s_0$. Regardless of the computational model, as indicated in Table 1, the order of the magnitude of maximum mean stress is roughly the same. The present results suggest that the magnitude of maximum mean stress for respective direction increases in the later stage of deformation.

The simplest craze yield condition for polymeric materials is given as $\sigma_1 - \sigma_3 \geq A + B / \sigma_m$ where σ_1 and σ_3 are the maximum and minimum principal stresses, respectively, and A and B are the temperature-dependent material constants (Sterstein et al., 1968). Out of necessity, the mean stress σ_m must be positive to develop a stress state favorable for crazing. Although the PC (polycarbonate) favors shear yielding, the positive mean stress in the matrix shown in Fig. 7 and Table 1 is an important characteristic value that governs the crazing of such materials as ABS (acrylonitrile-butadiene-styrene) and HIPS (high impact polystyrene) .

5.6 Effect of volume fraction of voids

In order to clarify the effect of volume fraction of voids on the deformation behavior of polymer containing voids, a simulation has been carried out for the case with void volume fraction $f_0 = 0.4$. Here, the obtained main results are summarized. Figure 9 shows the nominal stress and volumetric strain for unit cell versus nominal strain relationships for the polymer containing voids of sizes $r_1 / r_2 = 1, 2, 5$ and volume fraction $f_0 = 0.4$ under uniaxial tension with different tension directions $\theta = 0^\circ, 15^\circ, 30^\circ, 45^\circ$. Figure 10 indicates the typical

equivalent plastic strain rate distribution for the cases of $r_1/r_2 = 2$, $f_0 = 0.4$ and $\theta = 0^\circ, 15^\circ, 30^\circ, 45^\circ$. The macroscopic resistance of deformation remarkably decreases as the void volume fraction increases from 0.2 to 0.4. Interestingly, anisotropy in elastic response with respect to different tension directions is intensified as the void volume fraction increases for the case $r_1/r_2 = 1$, while almost isotropic response is seen for the case of heterogeneous voids with $r_1/r_2 = 2$. This tendency changes for $r_1/r_2 = 5$, which is attributable to the mode of deformation in the unit cell. The deformation behavior is almost completely controlled by the localized deformation connecting large voids. Therefore, the same situation discussed in 5.2 for $r_1/r_2 = 5$ is conformed. Regardless of the void volume fraction and heterogeneity, the evolution of volumetric strain for $\theta = 0^\circ$ ($\theta = 45^\circ$ for $r_1/r_2 = 5$) is almost identical. The magnitude of volumetric strain for $\theta = 15^\circ, 30^\circ, 45^\circ$ and their anisotropy with respect to tension direction increase with the volume fraction. However, as observed in Fig.3 (c), anisotropy in macroscopic response of polymer with voids increases as the heterogeneity of the voids increases.

With regard to the strain rate distribution, due to the reduction in the distance between the voids caused by the increase in the volume fraction of the voids the shear band connecting the voids becomes predominant. Nevertheless, the main characteristic feature of the shear band development is almost identical to that in the case of low volume fraction $f_0 = 0.2$. This tendency is also caused by the decrease in the stress concentration due to the increase in the radius of curvature of the voids. Indeed, the shear bands were much more localized within the ligament area regardless of the tension direction for the case of volume fraction $f_0 = 0.4$. The general pattern of the onset and propagation of shear bands is similar to that of the case with $f_0 = 0.2$.

Figure 11 shows the mean stress and strain rate distribution for the cases of $f_0 = 0.4$, $r_1/r_2 = 2$ and $\theta = 0^\circ, 30^\circ$. The concrete values of magnitude of local maximum mean stress is shown in Table 2. The comparisons between Figs. 8 and 11, and Tables 1 and 2 clarify that the decrease in volume fraction of moderately heterogeneous voids causes the increase in the value of local maximum mean stress over the macroscopic yielding range. Due to the concentration of deformation over the narrow ligament area, the maximum mean stress possesses high value for the case with high void volume fraction.

6. Conclusions

The problems associated with the tension-direction-dependent macro- to microscopic features of deformation of a polymer containing heterogeneous cylindrical voids that represent cavitated rubber particles, distributed periodically under the plane strain condition, have been investigated. A new homogenization method has been developed to solve the present problems. The onset and propagation of the shear band and the mean stress distribution in the polymer have been discussed in conjunction with the heterogeneity of the

voids and tension direction with respect to the principal direction of the unit cell. The results are summarized as follows.

(1) Depending on the tensile direction with respect to the unit cell, different types of shear bands are observed. The shear band connecting the voids, which appeared in the early stages of deformation causes softening and thus is associated with the decrease in the macroscopic yield stress. The onset of multiple shear bands contributes to relieving the localization of strain.

(2) Increasing the volume fraction of the voids causes yielding of the polymer matrix in the early stages of deformation so that the macroscopic yield stress and the directional dependence of the macroscopic stress-strain relationship decrease.

(3) The polymer with voids of moderately heterogeneous size shows complicated and different types of shear bands. Nevertheless, the macroscopic deformation behaviors are almost isotropic, which is due to the small voids that contribute to the high stress concentration, and promote the onset and propagation of the shear band.

(4) The dilatancy of the polymer with periodically distributed voids depends on the tension direction. In spite of complicated behavior of small voids due to the onset and propagation of shear bands, the volumetric change of large voids essentially governs the dilatancy of the polymer with voids.

(5) The decrease in the volume fraction of the voids causes an increase in the maximum value of the mean stress in the matrix around the macroscopic yielding range; while it is insensitive to the tension direction.

The present results, particularly those associated with the effect of heterogeneity of the voids and the tension directions on the micro- to macroscopic deformation behavior, provide new information. A quantitative discussion confirming the present results requires further 3D calculations. The present computational strategy may provide a computational tool for such 3D problems.

Acknowledgement

Financial support from the Ministry of Education, Culture, Sports, Science and Technology of Japan is gratefully acknowledged.

References

Argon, A. S., 1973. A theory for the low-temperature plastic deformation of glassy polymers. Phil. Mag. 28, 839-865.

Arruda, E. M. and Boyce, M. C., 1993. A three-dimensional constitutive model for large stretch behavior of rubber materials. J. Mech. Phys. Solids, 41, 389-412.

Arruda, E. M. Boyce, M. C., and Jayachandran, R., Effects of Strain Rate, Temperature and Thermomechanical Coupling on the Finite Strain Deformation Response of Glassy Polymers. Mechanics of Materials, 19, 193-212.

Boyce, M. C., Parks, D. M. and Argon, A. S., 1988. Large inelastic deformation of glassy polymers, Part I: rate dependent constitutive model. Mech. Mater., 7 , 15-33.

Fukui, T., Kikuchi, Y. and Inoue, T., 1991. Elastic-plastic analysis of the toughening mechanisms in rubber-modified nylon: matrix yielding and cavitation. Polymer, 32, 2367-2371.

Guedes, J. M. and Kikuchi, N., 1990. Preprocessing and postprocessing for materials based on the homogenization method with adaptive finite element solutions. Comput. Meth. Appl. Mech. Engng., 83, 143-198.

Hill, R., 1958. A general theory of uniqueness and stability in elastic-plastic solids. J. Mech. Phys. Solids, 10 , 236-249.

Kitagawa, H, Seguchi, Y. and Tomita, Y., 1972. An incremental theory of large strain and large displacement problems and its finite element application. Ing. Arch., 41, 213-224.

Ohno, N. and Okumura, D., 1999. On the formulation of homogenization methods of finite deformation in the updated Lagrangean form. Proc. JSME, 99.239-240(in Japanese).

Pijnenburg, K.G.W. and van der Giessen, E, 2001. Macroscopic yield in cavitated polymer blends. Int.J.Solids and Structures, 38 , 3575-3598.

Smit, R. J. M., Brekelmans, W. A. M. and Meijer, H. E. H., 1999. Prediction of the large-strain mechanical response of heterogeneous polymer systems: local and global deformation behavior of a representative volume element of voided polycarbonate. J. Mech. Phys. Solids, 47, 201-221.

Society of Polymer Science, Japan Eds.. 1991. High Performance Polymer Alloy, Maruzen Ltd., pp.215-237, (in Japanese)

Socrate, S. and Boyce, M. C., 2000. Micromechanics of toughened polycarbonate. J. Mech. Phys. Solids, 48, 233-273.

Steenbrink, A. C. and van der Giessen, E., 1997. Void growth in glassy polymer. J. Mech. Phys. Solids, 45 , 405-437.

Steenbrink, A. C. and van der Giessen, E., 1998. Strain localization and void growth in polymers. Proc. IUTAM Symposium on Materials Instabilities, De Borst, R. and van der Giessen, E., Eds., Wiley & Sons Ltd.. pp. 287-302,

Steenbrink, A. C. and van der Giessen, E., 1999. On cavitation, post-cavitation and yielding in amorphous polymer-rubber blends. J. Mech. Phys. Solids, 47, 843-876.

Sterstein, S. S., Ongchin, L. and Silverman, A., 1968. Inhomogeneous deformation and yielding of glasslike high polymers. Appl. Polym. Symp., 7 . 175-199.

Tanaka, S., Tomita, Y. and Lu, W., 2000. Computational simulation of deformation behavior of glassy polymer with cylindrical inclusion under tension. Trans. JSME., 66A, 454-463 (in Japanese).

Tomita, Y., and Tanaka, S., 1995. Prediction of deformation behavior of glassy polymers based on molecular chain network model. Int.J.Solids & Structures 32, 3423-3434

Tomita, Y., Adachi, T. and Tanaka, S., 1997. Modelling and application of constitutive equation for glassy polymer based on nonaffine network theory. Eur. J. Mech. A/Solids, 16 , 745-755.

Tomita, Y. and Adachi, T., 1998. Nonaffine network model for glassy polymer and prediction of instability propagation. Proc. IUTAM Symposium on Materials Instabilities, De Borst, R. and van der Giessen, E., Eds., Wiley & Sons Ltd.. pp.303-321,

Tomita, Y., Tanaka, S. and Lu, W., 1999. Constitutive equation of an amorphous polymer and its application to prediction of instability propagation behavior. Proc. ICM8, Progress in Mechanical Behaviour of Materials, Ellyin, F. and Provan, J.W., Eds., pp.1061-1066.

Tomita, Y. and Lu, W., 2001. Computational characterization of micro-to macroscopic mechanical behavior and damage of polymers containing second-phase particles. Int. J. Damage Mech., (in press)

Wu, P. D. and van der Giessen, E., 1993. On improved network models for rubber elasticity and their applications to orientation hardening in glassy polymers. J. Mech. Phys. Solids, 41 , 427-456.

Wu, X. and Ohno, N., 1999. A homogenization theory for inelastic behavior of materials with periodic internal structures. IUTAM Symposium on Micro- and Macrostructural Aspects of Thermoplasticity, Bruhns, O. T. and Stein E., Eds, Kluwer Academic Publishers. pp. 187-196,

Yee, A. F., 1977. The yield and deformation behavior of some polycarbonate blends. J. Mater. Sci., 12 , 757-765.

Figure Captions

Figure 1 Relation between macroscopic region and unit cell.

Figure 2 Computational model.

Figure 3 Nominal stress normalized by shear strength σ_t / s_0 and volumetric strain for unit cell E_v versus nominal strain u / L_0 for a polymer containing voids of sizes r_1 / r_2 =1, 2, 5 and volume fractions $f_0 = 0.2$. (a) r_1/r_2=1, (b)r_1/r_2=2, (c) r_1/r_2=5

Figure 4 Equivalent plastic strain rate normalized by average strain rate $\dot{\varepsilon}^p/\dot{\varepsilon}_0$ distributions corresponding to the cases in Figure 3. (a) r_1/r_2=1, (b) r_1/r_2=2, (c) r_1/r_2=5

Figure 5 Rotation and distortion of different sized voids under different directional tensions indicated by arrows for $f_0 = 0.2$. (a) r_1/r_2=1, (b) r_1/r_2=2, (c) r_1/r_2=5

Figure 6 Rotation angles α of different sized voids which initially aligned to tension directions for $f_0 = 0.2$. (a) θ=15^o (b) θ=30^o

Figure 7 Volumetric strain of voids e_v versus nominal strain u / L_0 for $f_0 = 0.2$. (a) r_1/r_2=1, (b) r_1/r_2=2, (c) r_1/r_2=5

Figure 8 Mean stress normalized by shear strength σ_m / s_0 and plastic strain rate normalized by average strain rate $\dot{\varepsilon}^p / \dot{\varepsilon}_0$ distribution in the matrix for $r_1 / r_2 = 2$, $f_0 = 0.2$.

Figure 9 Nominal stress normalized by shear strength σ_t / s_0 and volumetric strain for unit cell E_v versus nominal strain u / L_0 for a polymer containing voids of sizes r_1 / r_2 =1, 2, 5 and volume fractions $f_0 = 0.4$. (a) r_1/r_2=1, (b)r_1/r_2=2, (c) r_1/r_2=5

Figure 10 Equivalent plastic strain rate normalized by average strain rate $\dot{\varepsilon}^p/\dot{\varepsilon}_0$ distributions corresponding to the cases in Figure 9 for r_1/r_2=2.

Figure 11 Mean stress normalized by shear strength σ_m / s_0 and plastic strain rate normalized by average strain rate $\dot{\varepsilon}^p / \dot{\varepsilon}_0$ distribution in the matrix for $r_1 / r_2 = 2$, $f_0 = 0.4$.

Table Captions

Table 1 Maximum value of mean stress normalized by shear strength σ_m / s_0 in voids containing polymer for $f_0 = 0.2$.

Table 2 Maximum value of mean stress normalized by shear strength σ_m / s_0 in voids containing polymer for $f_0 = 0.4$.

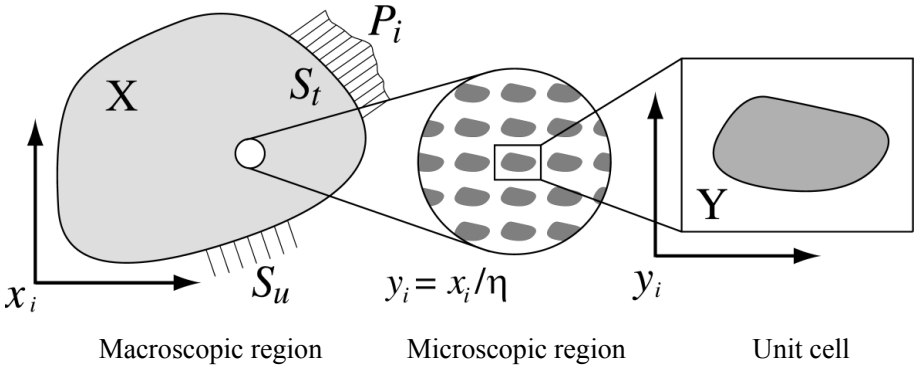

Figure 1 Relation between macroscopic region and unit cell.

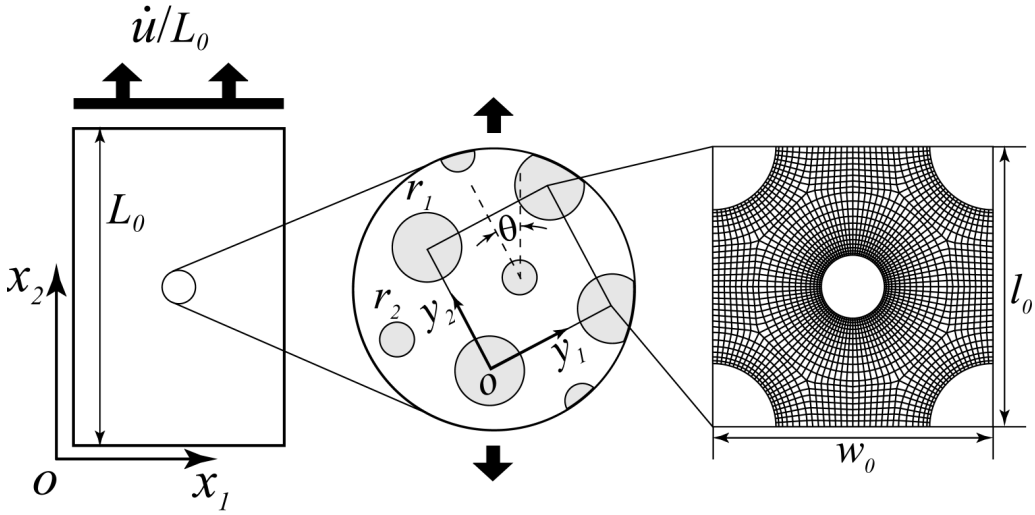

Figure 2 Computational model.

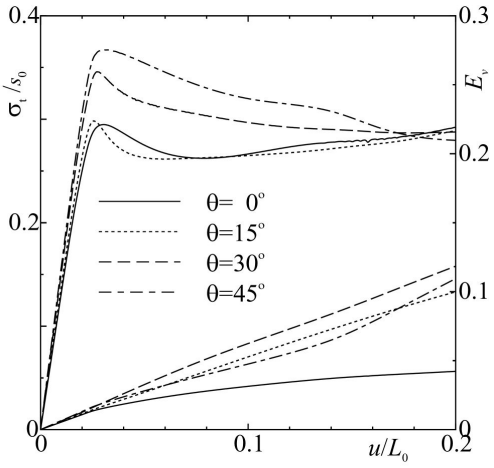

(a) $r_1 / r_2 = 1$

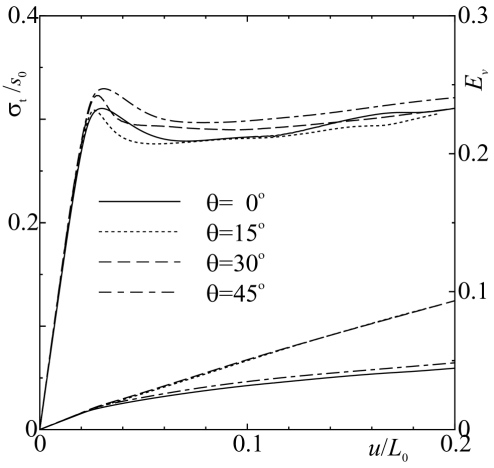

(b) $r_1 / r_2 = 2$

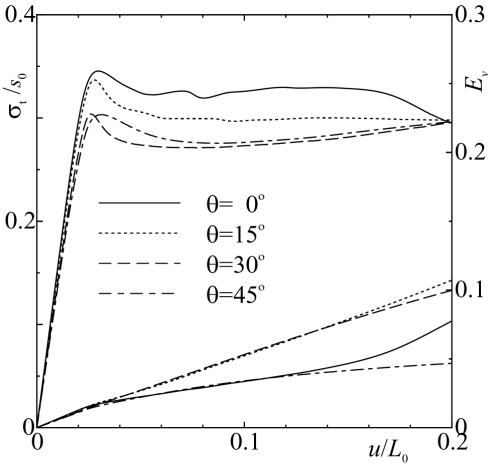

(c) $r_1 / r_2 = 5$

Figure 3 Nominal stress normalized by shear strength σ_t / s_0 and volumetric strain for unit cell E_v versus nominal strain u / L_0 for a polymer containing voids of sizes $r_1 / r_2 = 1,2,5$ and volume fractions $f_0 = 0.2$.

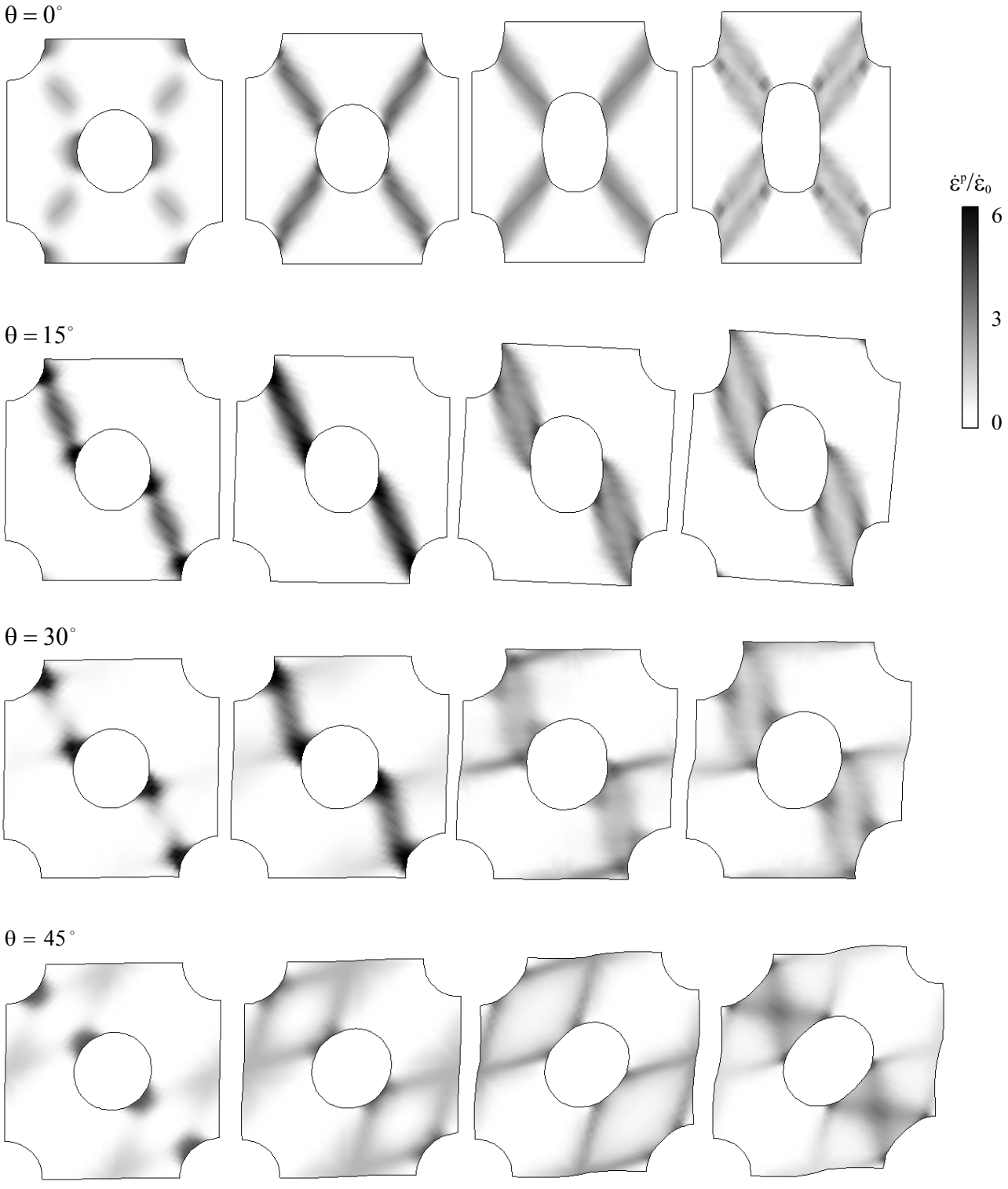
θ = 0°
θ = 15°
θ = 30°
θ = 45°
$\dot{\varepsilon}^p/\dot{\varepsilon}_0$
6
3
0
$u / L_0 = 0.025$
0.05
0.1
0.15

(a) $r_1 / r_2 = 1$

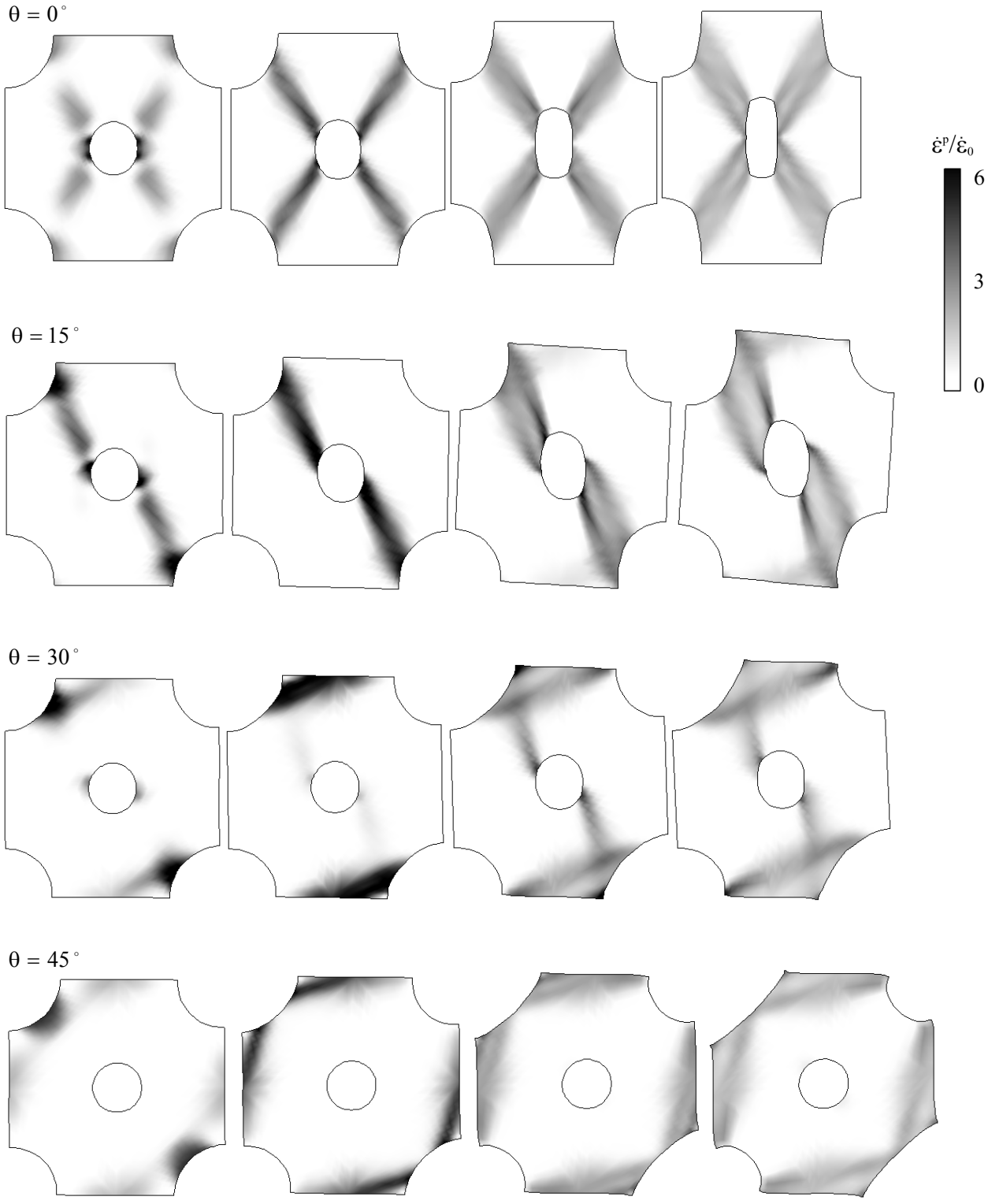
θ = 0°
θ = 15°
θ = 30°
θ = 45°
$\dot{\varepsilon}^p/\dot{\varepsilon}_0$
6
3
0
$u / L_0 = 0.025$
0.05
0.1
0.15

(b) $r_1 / r_2 = 2$

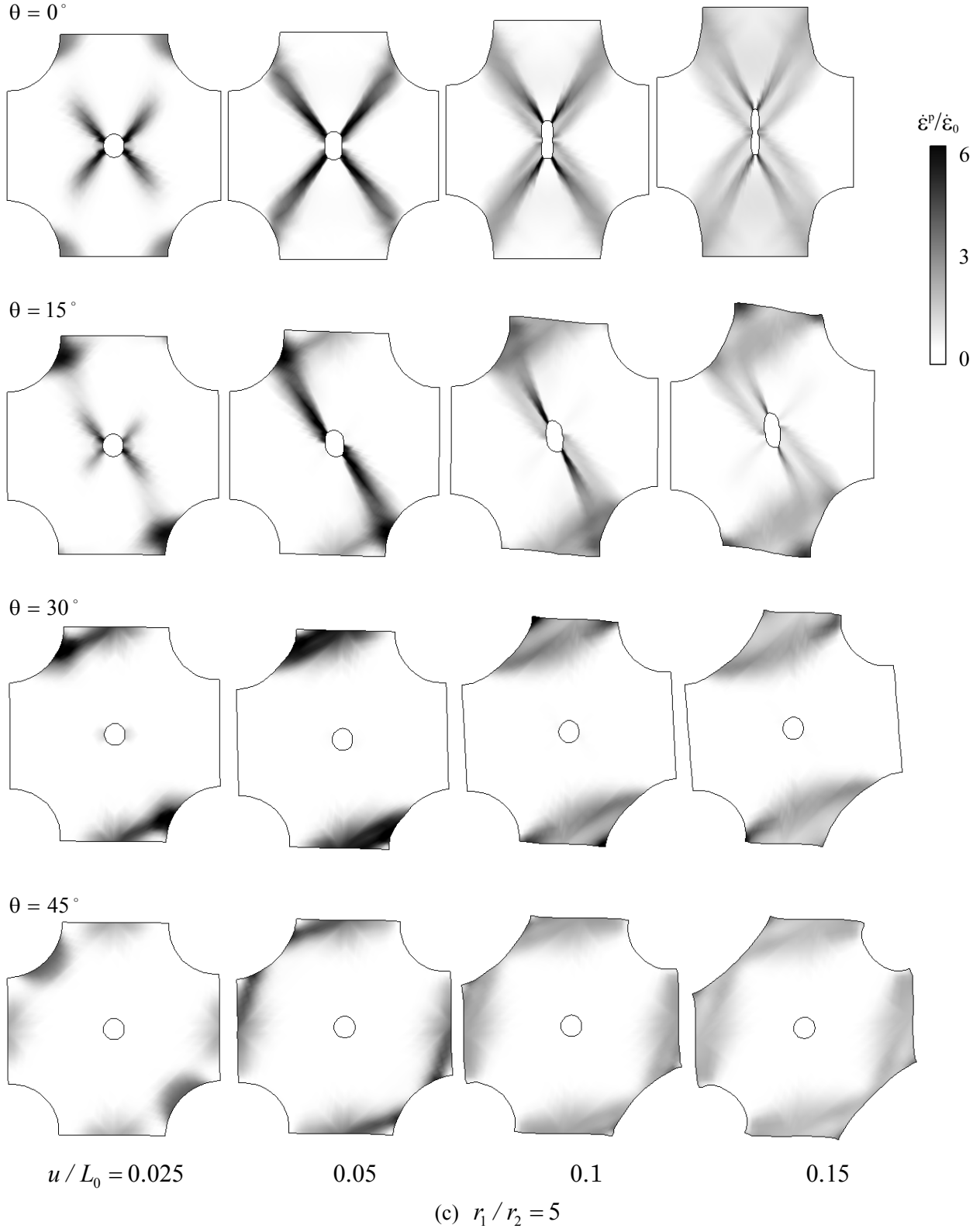

Figure 4 Equivalent plastic strain rate normalized by average strain rate $\dot{\varepsilon}^p/\dot{\varepsilon}_0$ distributions corresponding to the cases in Figure 3.

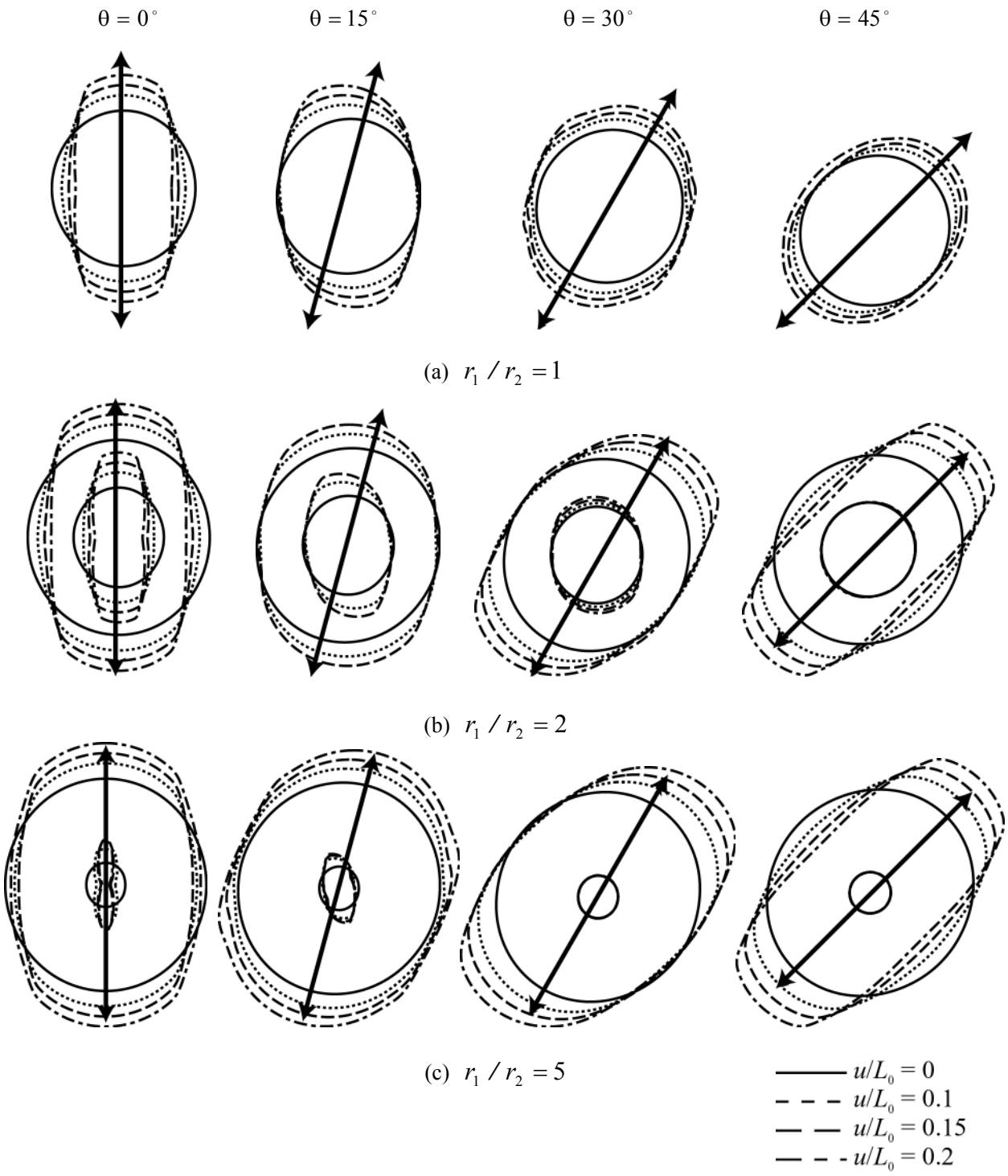

Figure 5 Rotation and distortion of different sized voids under different directional tensions indicated by arrows for $f_0 = 0.2$.

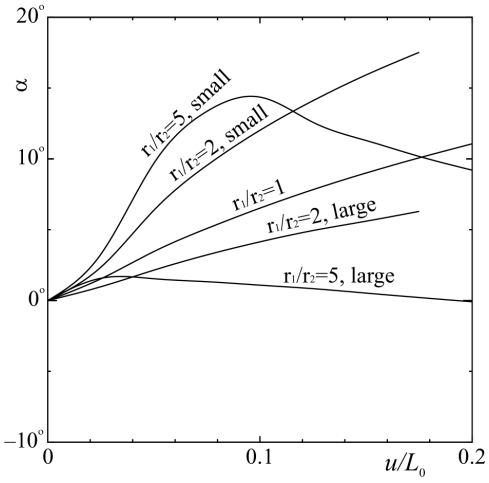

(a) $\theta = 15^\circ$

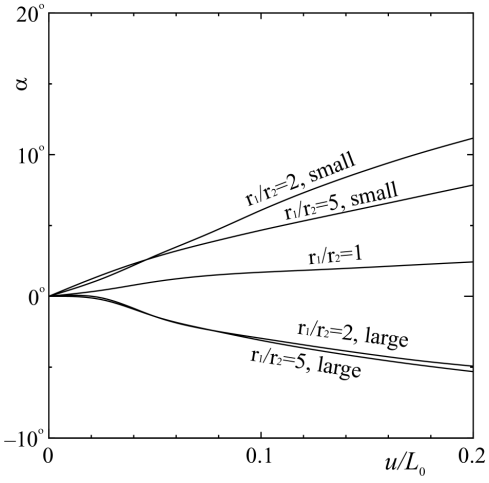

(b) $\theta = 30^\circ$

Figure 6 Rotation angles α of different sized voids which initially aligned to tension directions for $f_0 = 0.2$.

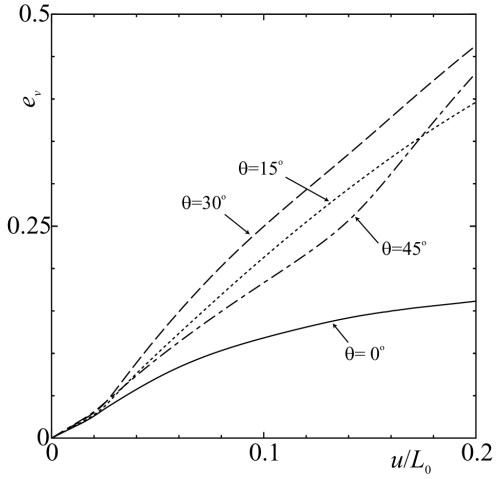

(a) $r_1 / r_2 = 1$

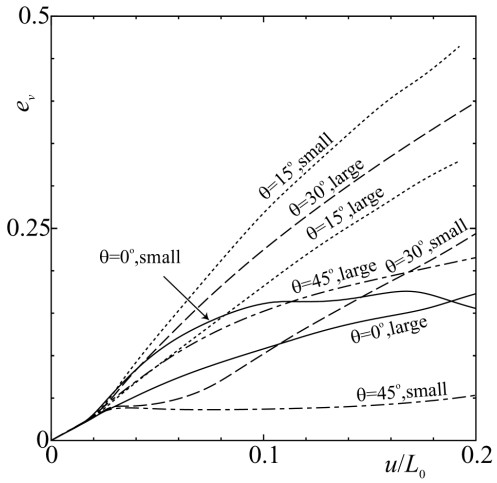

(b) $r_1 / r_2 = 2$

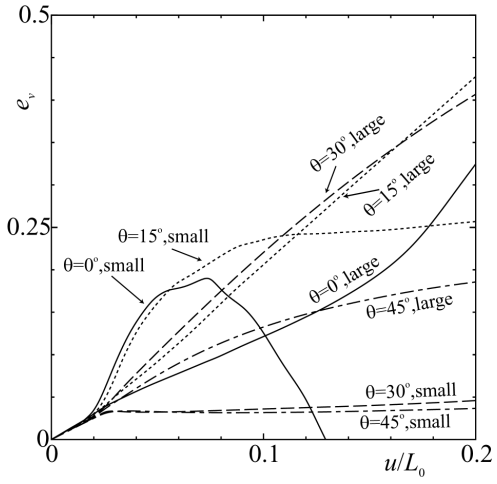

(c) $r_1 / r_2 = 5$

Figure 7 Volumetric strain of voids e_v versus nominal strain u / L_0 for volume fraction $f_0 = 0.2$.

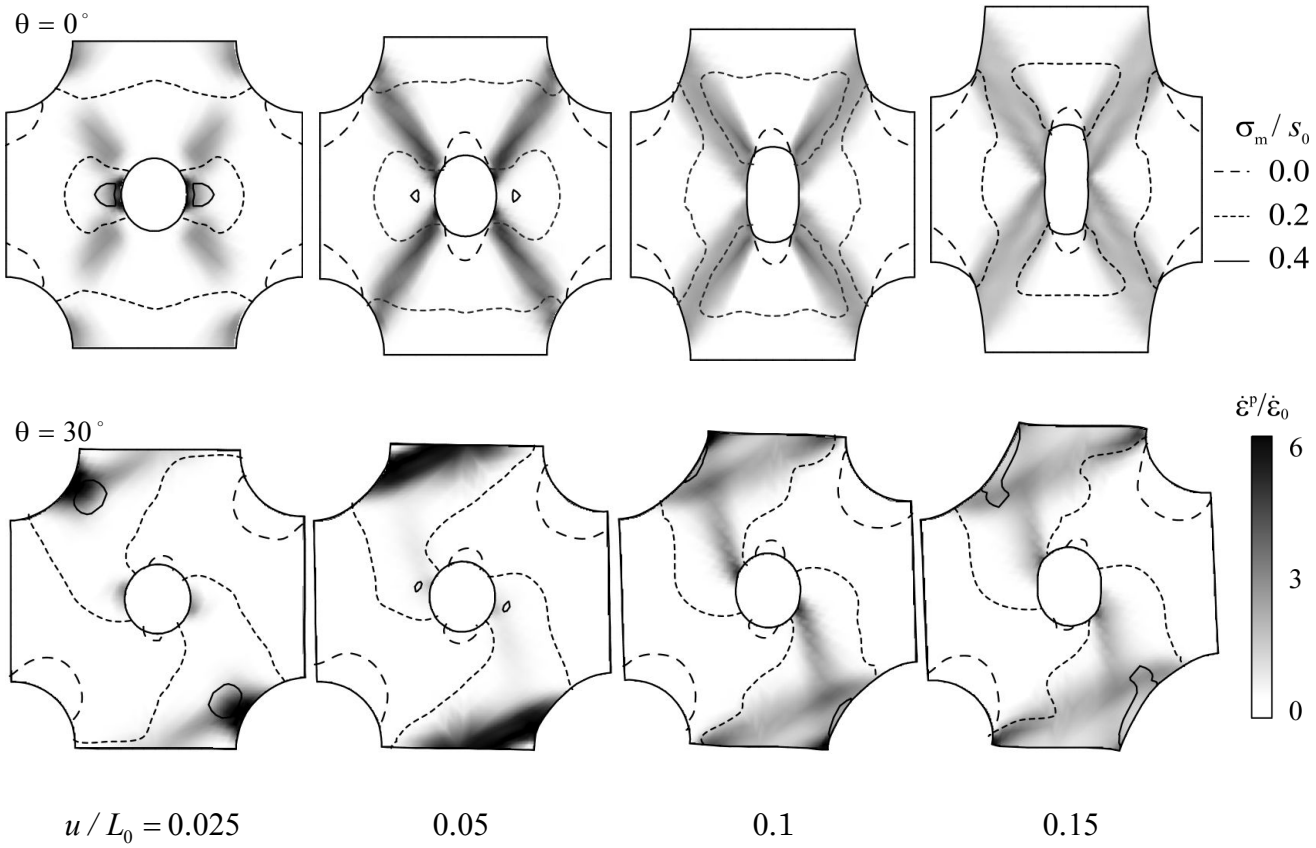

Figure 8 Mean stress normalized by shear strength σ_m / s_0 and plastic strain rate normalized by average strain rate $\dot{\varepsilon}^p / \dot{\varepsilon}_0$ distribution in the matrix for $r_1 / r_2 = 2$, $f_0 = 0.2$.

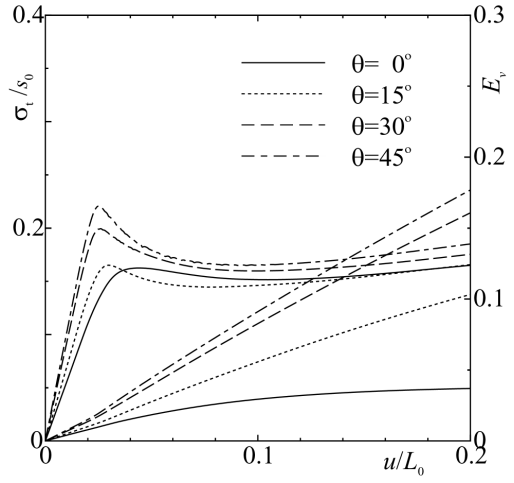

(a) $r_1 / r_2 = 1$

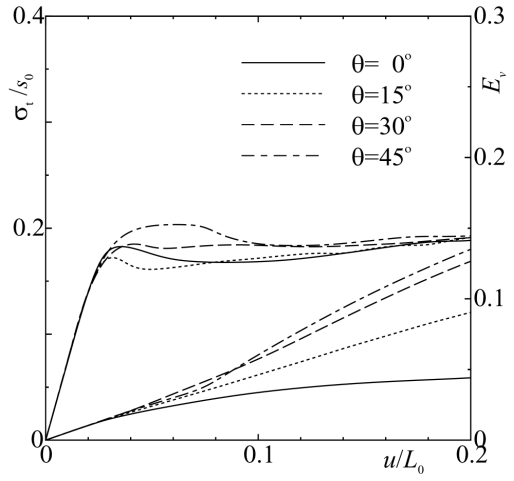

(b) $r_1 / r_2 = 2$

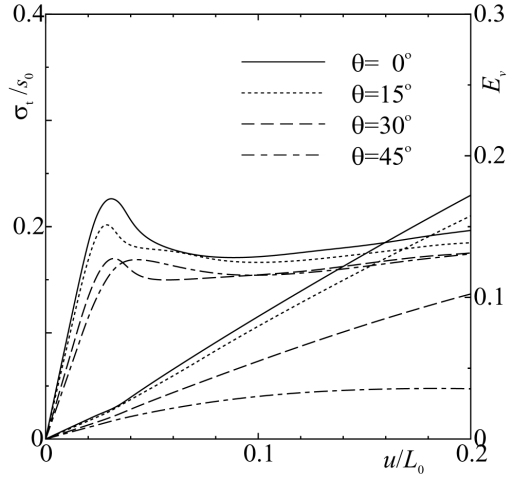

(c) $r_1 / r_2 = 5$

Figure 9 Nominal stress normalized by shear strength σ_t / s_0 and volumetric strain for unit cell E_v versus nominal strain u / L_0 for a polymer containing voids of sizes $r_1 / r_2 = 1,2,5$ and volume fractions $f_0 = 0.4$.

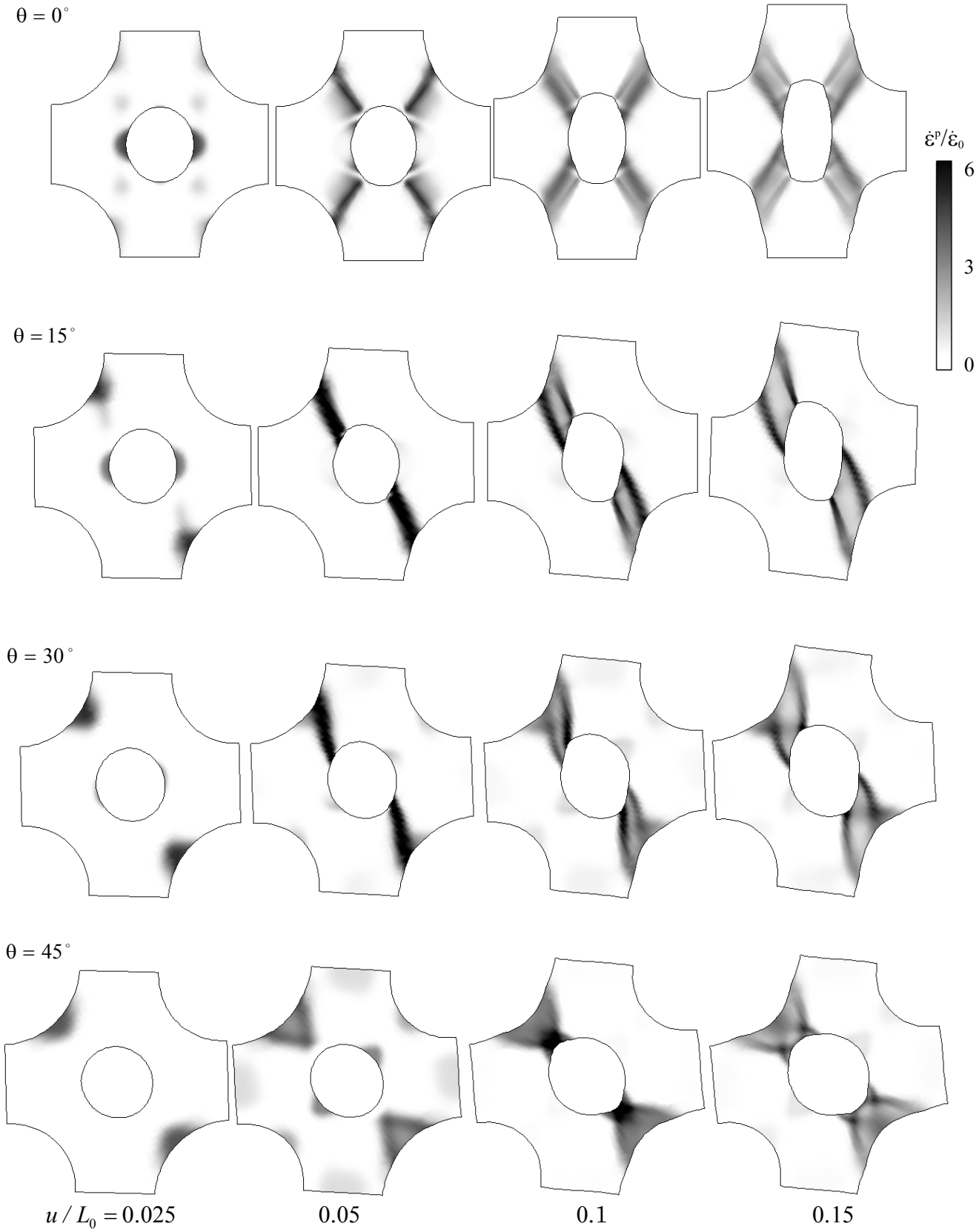

Figure 10 Equivalent plastic strain rate normalized by average strain rate $\dot{\varepsilon}^p/\dot{\varepsilon}_0$ distributions corresponding to the cases in Figure 9 for $r_1 / r_2 = 2$, $f_0 = 0.4$

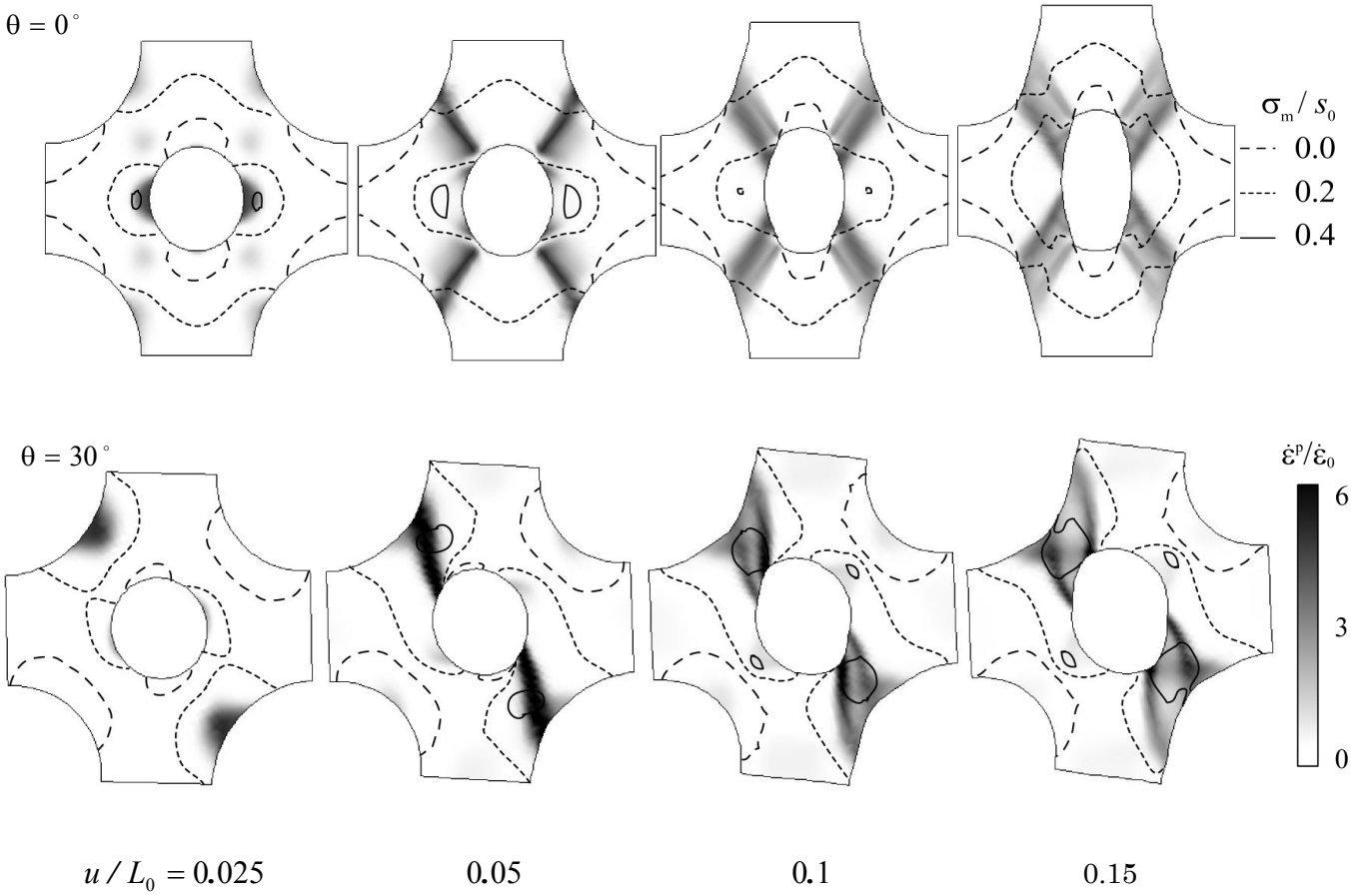

Figure 11 Mean stress normalized by shear strength σ_m / s_0 and plastic strain rate normalized by average strain rate $\dot{\varepsilon}^p / \dot{\varepsilon}_0$ distribution in the matrix for $r_1 / r_2 = 2$, $f_0 = 0.4$.

Table 1 Maximum value of mean stress normalized by shear strength σ_m / s_0 in voids containing polymer for $f_0 = 0.2$.

	u/L_0=	0.025	0.050	0.100	0.150	0.200
r_1/r_2=1	θ= 0°	0.452	0.401	0.363	0.347	0.381
	θ= 15°	0.477	0.405	0.449	0.491	0.606
	θ= 30°	0.492	0.554	0.536	0.532	0.556
	θ= 45°	0.462	0.510	0.469	0.506	0.491
r_1/r_2=2	θ= 0°	0.516	0.440	0.401	0.393	0.444
	θ= 15°	0.504	0.434	0.443	0.544	0.589
	θ= 30°	0.488	0.432	0.471	0.584	0.695
	θ= 45°	0.485	0.472	0.417	0.379	0.472
r_1/r_2=5	θ= 0°	0.483	0.447	0.454	0.496	0.469
	θ= 15°	0.491	0.448	0.490	0.529	0.612
	θ= 30°	0.474	0.425	0.444	0.514	0.628
	θ= 45°	0.464	0.444	0.395	0.366	0.372

Table 2 Maximum value of mean stress normalized by shear strength σ_m / s_0 in voids containing polymer for $f_0 = 0.4$.

	u/L_0=	0.025	0.050	0.100	0.150	0.200
r_1/r_2=1	θ= 0°	0.335	0.384	0.418	0.414	0.405
	θ= 15°	0.394	0.417	0.421	0.431	0.478
	θ= 30°	0.433	0.540	0.547	0.548	0.562
	θ= 45°	0.473	0.564	0.549	0.531	0.590
r_1/r_2=2	θ= 0°	0.442	0.463	0.424	0.436	0.397
	θ= 15°	0.403	0.419	0.521	0.450	0.482
	θ= 30°	0.426	0.465	0.568	0.596	0.630
	θ= 45°	0.405	0.566	0.578	0.613	0.628
r_1/r_2=5	θ= 0°	0.515	0.530	0.570	0.615	0.660
	θ= 15°	0.477	0.478	0.526	0.532	0.559
	θ= 30°	0.414	0.393	0.392	0.425	0.508
	θ= 45°	0.344	0.388	0.348	0.354	0.382